Chapter 3

Surface Fluxes of Momentum, Heat, and Water Vapor

John D. Albertson, University of California, Davis, CA
Gerard Kiely, University College Cork, Ireland
Marc B. Parlange, University of California, Davis, CA

Abstract

Advances in global scale hydrology and climatology demand an improved understanding of the interaction between the Earth's surface and its atmosphere. Such an understanding is being sought through field experiments over the ocean and the land and through the use of remote sensing. In many cases, the traditional eddy correlation measurement technique to obtain fluxes of heat and momentum is problematic and it becomes necessary to employ less direct techniques. In this paper the inertial-dissipation method is reviewed and a refined approach is presented. The new dissipation model circumvents several of the short-comings inherent to previous formulations of the dissipation approach. Experimental data are presented to support new empirical scaling forms for turbulent kinetic energy and scalar variance dissipation rates and the refined dissipation-flux model is tested. Excellent agreement with direct flux measurements is obtained.

3.1 Introduction

Momentum and scalar fluxes between the Earth's surface and its atmosphere are fundamental to issues ranging from watershed management to climate systems, as well as to our basic understanding of flow and transport in the atmospheric surface layer. Efforts to model the atmospheric boundary layer (ABL) in itself or as part of a larger climate simulation model are limited by an inadequate understanding of surface fluxes over the land and the ocean. Advances in regional and global scale hydro-meteorology must rely on observations of the exchange between the Earth's surface and its atmosphere. For these observations to be relevant, they must be made over a spatial scale appropriate to the problem being addressed. Satellite-based instruments hold promise for diagnosing and mapping surface fluxes. However, the development of reliable algorithms for relating the instrument readings to actual surface fluxes hinges on a program of careful comparison of algorithm estimates to actual measurements of the fluxes. Benchmark flux measurements may be acquired through (i) inference from vertical

profiles of mean meteorological quantities using Monin-Obukhov similarity theory, (ii) remote sensing of ABL turbulence with lidar or scintillometry, or (iii) *in situ* point measurements of turbulent fluxes using eddy correlation or dissipation techniques in the ABL. For these techniques to provide measurements that represent integrated fluxes over large spatial scales, the measurements must be made above the blending height; here we rely on the thorough mixing provided by the extremely high Reynolds number turbulent flow of the ABL. For a complete discussion of the idea of a blending height and the relationship between measurement height and spatial integration of surface fluxes see the recent review paper by Parlange et al. (1995b).

Although the eddy correlation (EC) method provides a direct measurement of the vertical fluxes, there are applications for which it is inappropriate, particularly over water and for remote field experiments requiring long term unattended operation. Fluxes from the mean profile method or the bulk aerodynamic method have limitations as well. The flux-dissipation method is used widely over water surfaces, typically using power spectra to determine the dissipation rates, followed by an iterative procedure to determine fluxes. However, this approach suffers from uncertainties due to empirical inertial subrange constants, the jumpy (or noisy) nature of power spectra, and the reliance on an iterative solution. In this paper we introduce a one-step (non iterative) dissipation method for determining fluxes of momentum, sensible heat and water vapor. This new method which uses third order structure functions to determine dissipation rates, avoids many of the pitfalls previously assumed unavoidable with the dissipation method. The results presented here may also improve the reliability of flux estimates from the ABL remote sensing instruments, such as lidar and scintillometers, since these techniques typically rely on an empirical relationship between scalar fluxes and the dissipation rate of scalar variances (see Hill et al., 1992 and Eichinger et al., 1993).

3.1.1 The Atmospheric Boundary Layer

The ABL is that layer of air, directly above the Earth's surface in which the effects of the surface (friction, evaporation, heating and cooling) are felt directly on time scales less than a day. The ABL is broadly made up of two layers, the atmospheric surface layer (ASL) and the mixed layer (ML). The ASL is affected primarily by surface fluxes while the ML is affected by both surface fluxes and boundary layer entrainment of the free atmosphere air from above. Figure 3.1 is a schematic of the composition of the ABL. The ASL occupies about the lowest 10% of the fully developed daytime ABL, or approximately the first 100 m above the Earth's surface (Parlange et al., 1995b).

In the ASL, the turbulent flow is often assumed to be statistically stationary, when considering periods of 10 minutes to 1 hour. The principle mechanism for the mechanical production of turbulence in this time period is the vertical gradient of the mean wind. Figure 3.2 shows schematics of the vertical profiles of the means of velocity U, potential temperature Θ, and humidity $\overline{q}$ for the daytime convective boundary layer (CBL). It is seen from Figure 3.2, that the steepest gradients occur in the lower 10% of the boundary layer (i.e. the ASL), while in the upper 90% of the CBL strong convective mixing and entrainment of the free atmosphere air at the top of the ABL smooth out almost all vertical variations in the mean profiles.

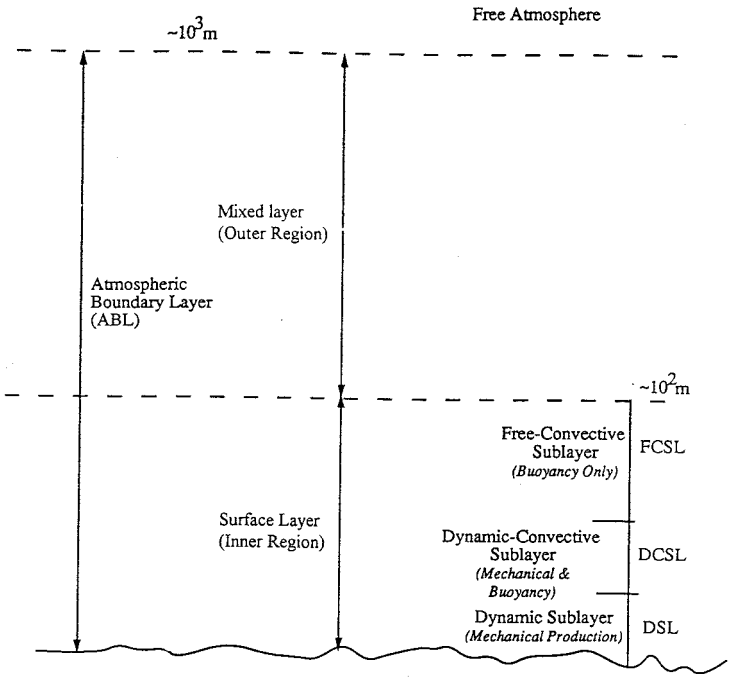

Figure 3.1: *Atmospheric boundary layer schematic.*

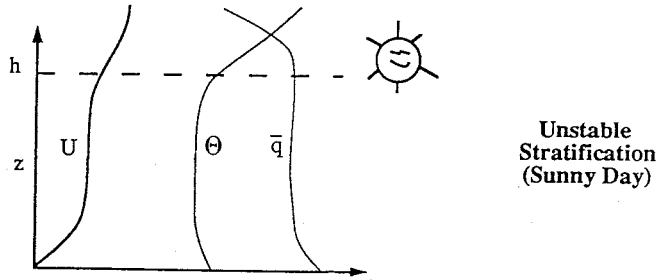

Figure 3.2: *Mean profiles of wind speed, potential temperature, and humidity in the convective atmospheric boundary layer.*

3.1.2 Surface Layer Scaling

ASL Turbulence

Before getting into the details of ASL scaling, it is instructive to review briefly the turbulence spectrum as shown schematically in Figure 3.3. The eddies carrying most of the energy are of the larger, integral scale size. The integral scale for longitudinal velocity (defined by l)

is representative of the large, turbulent energy producing eddies. At the other end of the spectrum, energy is dissipated by molecular viscosity via eddies of length scale approaching the Kolmogorov scale η (typically of order $\approx$ 1 mm). Between these two extremes lies what is known as the inertial subrange, which marks the broad range of scales between the anisotropic energy bearing eddies and the viscosity controlled dissipative eddies. This inertial range, for high Reynolds number flows as found in the ASL, spreads over several orders of magnitude of wavenumbers. Referring to Figure 3.3, the spectral density peaks at wavenumbers of the order of l^{-1} . For the mid-spectrum inertial scales, Kolmogorov (1941) postulated that the energy content is controlled simply by the eddy size (k) and the rate of energy transfer through the spectrum (taken under an assumption of steady state as ε, the average dissipation rate of turbulent kinetic energy). Consequently, straight dimensional analysis yields Kolmogorov's celebrated -5/3 spectrum for the inertial subrange, $E(k) \sim \varepsilon^{2/3}k^{-5/3}$. It is seen from Figure 3.3, that as k increases, the energy falls with a slope of -5/3 (in a log-log framework). For wavenumbers approaching η^{-1}, local dissipation induces steadily faster decay of energy content. We make much use of Kolmogorov's relationship in later sections.

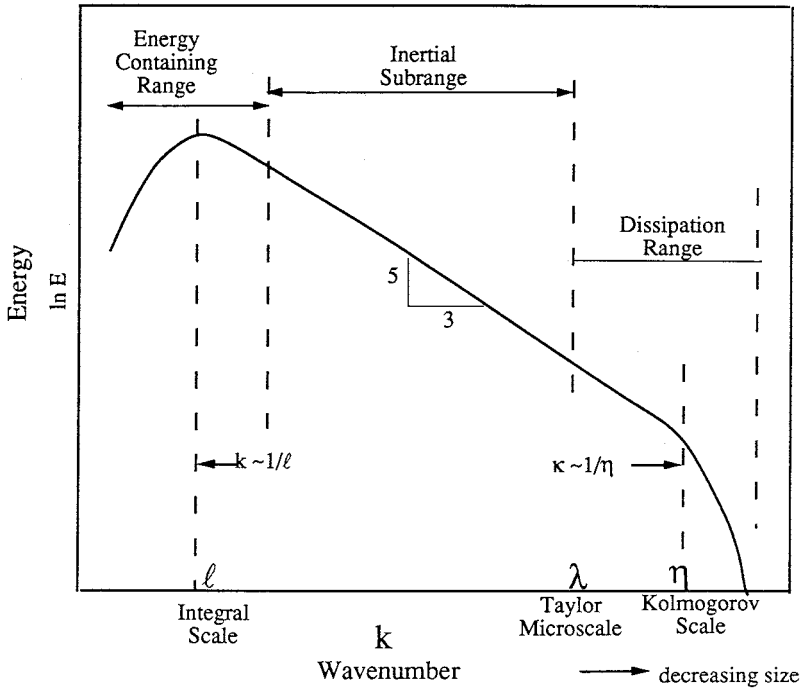

Figure 3.3: *Schematic of the power spectrum. The integral length scale is represented by l and the Kolmogorov length scale is represented by η. Wavenumbers (k) are in radians/length.*

Turbulence due to the gradient of the mean wind speed is created by mechanical (shear) turbulence. A second form of turbulence production is that due to buoyancy, induced by vertical temperature stratification. In general, turbulence is produced by a combination of both during daytime hours, with the ratio of buoyant to mechanical production of turbulence increasing

with height. This ratio is represented by the stability parameter, $-z/L$, where z is the height above the surface and L is the Monin-Obukhov length

$$L = -\frac{u_*^3\Theta}{kg < w\theta >} \tag{3.1}$$

where the friction (shear) velocity is u_*, the fluctuating vertical velocity is w, the mean potential air temperature is Θ and its fluctuating component is θ, the dimensionless parameter k is von Karman's constant ($\simeq$ 0.4) and g is gravitational acceleration. The three classifications of atmospheric stability can be expressed in terms of the stability parameter as

$$\begin{aligned} &unstable \;\; stratification & -\frac{z}{L} &> 0 \\ &neutral & -\frac{z}{L} &\Rightarrow 0 \\ &stable & -\frac{z}{L} &< 0 \end{aligned} \tag{3.2}$$

Monin-Obukhov Scaling

Prandtl set out the concept of the logarithmic wind velocity profile, based on dimensional analysis. In plane parallel flow, an increase of the horizontal mean velocity in the z direction is evidence of a downward momentum flux. Thus the gradient of mean velocity is determined by the shear stress at the earth surface, and the distance from that surface, such that

$$\frac{dU}{dz} = \frac{u_*}{kz} \tag{3.3}$$

Upon integration from z_1 to z_2 we obtain the familiar log law

$$U_2 - U_1 = \frac{u_*}{k}\ln\left(\frac{z_2}{z_1}\right) \tag{3.4}$$

where U_1 and U_2 are the mean longitudinal velocities at elevations z_1 and z_2.

The similarity theory of Monin and Obukhov extended Prandtl's scaling to scalars and into the unstable and stable regimes. This was accomplished by noting the analogy between scalars and velocity and by admitting additional variables to the dimensional analysis to account for the effect of density stratification (i.e. (3.1)). Monin-Obukhov (MO) scaling of mean profiles in the ASL, for example, yields

$$\frac{dU}{dz} = \frac{u_*}{kz}\Phi_m\left(\frac{z}{L}\right) \tag{3.5a}$$

$$\frac{d\Theta}{dz} = \frac{\Theta_*}{kz}\Phi_H\left(\frac{z}{L}\right) \tag{3.5b}$$

$$\frac{d\overline{q}}{dz} = \frac{q_*}{kz}\Phi_q\left(\frac{z}{L}\right) \tag{3.5c}$$

with $\Theta_*(= -H/\rho c_p u_*)$ being a temperature scale, $q_*(= -E/\rho u_*)$ a humidity scale, and Φ_m, Φ_H, and Φ_q representing non-dimensional gradients of mean velocity, temperature, and humidity, respectively. A basic premise of MO scaling is that the stability functions (e.g. Φ_m, Φ_H, and Φ_q) are universal functions of the stability parameter.

Recently a three sublayer model has been proposed as an extension of MO scaling (see Kader, 1988, and Kader and Yaglom, 1990). This model represents the lowest sublayer of the ASL

as the *Dynamic Sublayer* (DSL) in which buoyant action is negligible compared to mechanical production. The uppermost sublayer of the ASL, governed by buoyancy only, is termed the *Free Convection Sublayer* (FCSL). Between these two is a sublayer, driven by both mechanical and buoyant forces, termed the *Dynamic-Convective Sublayer* (DCSL). The sublayers are separated by narrow regions of transition. The $-z/L$ limits of the sublayers, based on the order of magnitude analysis of Kader (1992), are

$$\begin{aligned} DSL &: \quad -z/L < 0.04 \\ DCSL &: \quad 0.12 < -z/L < 1.2 \\ FCSL &: \quad -z/L > 2.0 \end{aligned}$$

The TKE and temperature variance budget equations are scaled in the context of the three sublayer model using directional dimensional analysis (DDA) which involves different length scales for the different directions, with L_x for the horizontal and L_z for the vertical (see Panton, 1984, p.207–209). The use of DDA implies that the vertical and horizontal motions are uncoupled. In the DCSL the energy transferred between the horizontal and vertical motions through vortex stretching is considered to be much less than that produced in each the vertical and horizontal directions. Therefore, the transfer between directions is ignored and we consider the horizontal motions to be driven solely by horizontal processes (shear) and the vertical motions to be driven solely by vertical processes (buoyancy) only. We will return to this model below as we examine the scaling of the TKE and scalar variance budget equations. For further review of DDA and its application to dissipation rates see Albertson et al. (1996).

Fluxes and methods of determination

The vertical fluxes of momentum, heat and moisture are defined as

$$u_* = [- < uw >]^{1/2} \tag{3.6a}$$

$$H = \rho c_p < w\theta > \tag{3.6b}$$

$$E = \rho < wq > \tag{3.6c}$$

where q is the fluctuation from the mean specific humidity and ρ is the mean air density. The latent heat flux (LE) is related to the evaporation rate (E) as $LE = L_v E$, where L_v is the latent heat of vaporization of water (see Brutsaert, 1982).

The four standard techniques of flux determination are eddy correlation, mean profiles, bulk aerodynamic, and inertial-dissipation (see Brutsaert, 1982). The eddy correlation (EC) method is a direct measurement of fluxes, while the other three are indirect methods relying on similarity theory. The EC method requires the measurement of the fluctuating components of the vertical velocity, and an associated fluctuating component for the term being transported, e.g.: horizontal velocity, for momentum flux; temperature, for heat flux; and humidity, for moisture flux. The use of EC on a moving platform (ship or aircraft) is prone to errors due to contamination of the w signal by motion of the platform. The mean profile method requires precise measurements of the vertical gradients of the mean meteorological variables, which is also difficult when applied from ships or aircraft. The bulk aerodynamic method is largely a conceptual approach consisting of bulk transfer equations with drag coefficients which are estimated experimentally (Brutsaert, 1982, p.201; Brutsaert, 1986). The dissipation approach is significantly less susceptible to errors from ship motion, but does require measurement of turbulent fluctuations at a frequency capable of resolving fluctuations in the inertial subrange as well as the use of similarity theory and other assumptions in its formulation. With this last approach the fluxes (covariances) are not determined directly but are derived from turbulence measurements and use of variance budget equations that relate surface fluxes to mean dissipation rates. Therefore, we begin the discussion of this method with an examination of the budget equations for turbulent kinetic energy and temperature variance (with temperature serving as a proxy for any other scalar).

3.1.3 Turbulent kinetic energy

The mean turbulent kinetic energy (TKE) dissipation rate (ε) is related to the production rate of TKE and hence the surface fluxes through the TKE budget equation. The TKE budget equation is obtained by multiplying the momentum equation for the $\alpha(= 1,2,3)$ direction, by u_α, time averaging all terms and subtracting the equation governing the kinetic energy of the mean flow (Tennekes and Lumley, 1972, p63). For a stationary flow with horizontal homogeneity we write the budget equation for the time averaged TKE per unit mass with the Boussinesq approximation as

$$- < uw > \frac{\partial U}{\partial z} + \frac{g < w\theta >}{\Theta} - \frac{1}{2}\frac{\partial < ew >}{\partial z} - \frac{1}{\rho}\frac{\partial < pw >}{\partial z} = \varepsilon \tag{3.7}$$

where p is the fluctuating component of the pressure, and e is twice the TKE (i.e. TKE $=\frac{e}{2} = \frac{u^2+v^2+w^2}{2}$). The first term in (3.7) represents the mechanical (or shear) production of TKE by interaction of the Reynolds stress with the mean velocity gradient. The second term represents the TKE production by buoyancy, the third the divergence of vertical turbulent flux of TKE and the fourth the transfer term for TKE due to pressure-velocity interaction. The latter two terms on the left hand side of (3.7) are generally called the transport terms. This budget is non-dimensionalized by u_*^3/kz to arrive at

$$\Phi_m\left(\frac{z}{L}\right) - \frac{z}{L} - \frac{Fkz}{u_*^3} - \frac{Pkz}{u_*^3} = \Phi_\varepsilon\left(\frac{z}{L}\right) \tag{3.8}$$

where

$$\Phi_\varepsilon\left(\frac{z}{L}\right) = \frac{\varepsilon kz}{u_*^3} \tag{3.9}$$

and F and P are written for $\frac{1}{2}\frac{\partial < ew >}{\partial z}$ and $\frac{1}{\rho}\frac{\partial < pw >}{\partial z}$, respectively.

It is often assumed that total production (mechanical plus buoyant) equals dissipation (Deacon, 1988), regardless of the state of atmospheric stratification and position in the boundary layer, i.e.

$$\Phi_m - \frac{z}{L} \approx \Phi_\varepsilon \tag{3.10}$$

where Φ_m is the dimensionless mechanical production and $-z/L$ is the dimensionless buoyant production.

In the Kansas experiments, Wyngaard and Coté (1971; abbreviated here as WC71) made measurements of the production, turbulent transport and dissipation of TKE for near neutral and moderately unstable stratification. Their results showed dissipation exceeding production

for the slightly unstable flows, with an equality approached for more strongly convective flows. Their empirical functions for non-dimensional shear production and dissipation are

$$\Phi_m\left(\frac{z}{L}\right) = \left(1+16\left|\frac{z}{L}\right|\right)^{-\frac{1}{4}} \tag{3.11a}$$

$$\Phi_\varepsilon\left(\frac{z}{L}\right) = \left(1+0.5\left|\frac{z}{L}\right|^{\frac{2}{3}}\right)^{\frac{3}{2}} \tag{3.11b}$$

WC71 suggested that the pressure-velocity term may be important but that direct measurements were needed to investigate this. Work by McBean et al. (1971) also found dissipation to exceed total production for $-z/L > 0.3$. Further work by McBean and Elliot (1975) in measurements of F and P over dry prairie land showed that these two terms were somewhat balanced, with P adding energy and F removing energy. Leavitt and Paulson (1975) in an ocean experiment concluded that dissipation equalled production. Champagne et al. (1977), in work over bare furrowed soil, found dissipation to exceed production. Frenzen and Vogel (1992), in an experiment over wheat in Wyoming, found the dissipation rate to be less than production and showed that with corrections the WC71 data show dissipation equalling production. Many of these studies represent narrow ranges of stability. Yet, the different circumstances and measurement techniques of the studies inhibit the drawing of conclusions from the studies taken as an ensemble. Therefore, we present new experimental results from dissipation measurements made over a wide range of stability (Albertson et al., 1996; Kiely et al., 1996) and we investigate the scaling of these measurements in the context of the three sublayer model.

Accepting that all one point fluctuation moments in the DSL are independent of z (Kader, 1992), then F and P vanish in this region. Therefore, in the DSL the normalized dissipation rate should equal the normalized production rate, which is know to be a constant of order 1.0. In the DCSL the F and P terms may be significant. From DDA the shear velocity u_* has dimensions of $L_x^{1/2}L_z^{1/2}t^{-1}$ and the convective velocity $w_*(=[<w\theta>gz/\Theta]^{1/3})$ has dimensions of $L_z t^{-1}$, where t is used to represent the time dimension. The convective velocity is used to scale the vertical motion and the combination u_*^2/w_* is used to scale the horizontal motions. In the FCSL the scaling is independent of u_* and thus the relevant velocity is w_*. From dimensional analysis for the TKE we obtain (Albertson et al., 1996)

$$\Phi_\varepsilon = \Phi_m = C_1 \approx 1 \qquad -\frac{z}{L} < 0.04 \tag{3.12a}$$

$$\Phi_\varepsilon = C_2\left(-\frac{z}{L}\right)^{-\frac{1}{3}} + C_3\left(-\frac{z}{L}\right) \qquad 0.12 < -\frac{z}{L} < 1.2 \tag{3.12b}$$

$$\Phi_\varepsilon = C_4\left(-\frac{z}{L}\right)^{\frac{1}{3}} + C_5\left(-\frac{z}{L}\right) \qquad -\frac{z}{L} > 2.0 \tag{3.12c}$$

In the DCSL, C_2 is a constant that describes the effects of mechanical production and the vertical transport of $<u^2>$ and $<v^2>$. The value of C_3 accounts for the buoyant production and the combined effects of vertical transport of $<w^2>$ and the pressure-velocity interaction (Kader, 1992). In the FCSL, C_4 describes the contribution of shear production, and C_5 represents that due to buoyancy and the transport contributions F and P. Since shear production is negligible in the FCSL, the C_4 term may be neglected in practice (i.e. $C_4 \to 0$). The constants in (3.12) are determined below by regression fit to the experimental results of Albertson et al. (1996).

3.1.4 Temperature variance

The mean dissipation rate of the temperature variance (ε_θ) is related to the vertical temperature flux ($<w\theta>$) through the temperature variance budget equation, (actually the budget for $\frac{1}{2}<\theta^2>$), which for steady, horizontally homogenous flow is written

$$-<w\theta>\frac{\partial\Theta}{\partial z} - \frac{1}{2}\frac{\partial <w\theta^2>}{\partial z} = \varepsilon_\theta \tag{3.13}$$

The first term is the average rate of production of temperature variance by interaction of the vertical heat flux with the vertical gradient of mean potential temperature. The second term represents the flux divergence of the variance. Non-dimensionalizing (3.13) by $u_*\Theta_*^2/kz$ yields

$$\Phi_H\left(\frac{z}{L}\right) - \frac{kz}{u_*\Theta_*^2}T_r = \Phi_{\varepsilon_\theta}\left(\frac{z}{L}\right) \tag{3.14}$$

where T_r $(=\frac{1}{2}\frac{\partial<w\theta^2>}{\partial z})$ is the dimensional transport, Φ_H is the dimensionless production of temperature variance from (3.5), and $\Phi_{\varepsilon_\theta}(=\frac{\varepsilon_\theta kz}{\Theta_*^2 u_*})$ represents the dimensionless dissipation rate of temperature variance. Hogstrom (1990) found measurements of the transport term to contain large scatter, as with WC71, but found no systematic deviation from zero.

The classic Businger-Dyer empirical formula for the normalized production in the near neutral and unstable region is (Businger, 1966; Dyer, 1967)

$$\Phi_H = \left(1+16\left|\frac{z}{L}\right|\right)^{-\frac{1}{2}} \qquad \text{for} \qquad 0 < -\frac{z}{L} < 2 \tag{3.15}$$

although the empirical constants are subject to some uncertainty and varying interpretation. However, several recent studies have found that Φ_H scales convectively (i.e. $\propto (-z/L)^{-\frac{1}{3}}$) for $-z/L \gg 0$ (e.g. Kader and Perepelkin, 1984). An important point is that under convective scaling, $\Phi_{\varepsilon_\theta}$ is also proportional to $(-z/L)^{-\frac{1}{3}}$, and hence ε_θ is independent of surface shear stress. This simplifies greatly the calculation of H from ε_θ.

Following the approach described above for the three sublayer model we obtain the following scaling form for the temperature variance dissipation

$$\Phi_{\varepsilon_\theta} = \Phi_H = B_1 \approx 1 \qquad -\frac{z}{L} < 0.04 \tag{3.16a}$$

$$\Phi_{\varepsilon_\theta} = B_2\left(-\frac{z}{L}\right)^{-\frac{1}{3}} \qquad 0.12 < -\frac{z}{L} < 1.2 \tag{3.16b}$$

$$\Phi_{\varepsilon_\theta} = B_3\left(-\frac{z}{L}\right)^{-\frac{1}{3}} \qquad -\frac{z}{L} > 2. \tag{3.16c}$$

Note that the production and dissipation rates scale with $(-z/L)^{-1/3}$ for all but the most neutral region of the convective boundary layer, and not with $(-z/L)^{-1/2}$ as was suggested in earlier research (e.g. WC71). This -1/3 scaling simplifies greatly the process by which heat fluxes are computed from inertial subrange measurements of scalar dissipation rates. The constants in (3.16) are determined below from the results of recent experiments (Kiely et al., 1996).

3.1.5 Computing fluxes from dissipation rates

From the dimensionless dissipation functions Φ_ε and $\Phi_{\varepsilon_\theta}$ and measurements of ε and ε_θ we may estimate the momentum and heat fluxes. The u_* and H estimates may be determined from

$$u_* = \left[\frac{kz\varepsilon}{\Phi_\varepsilon\left(\frac{z}{L}\right)}\right]^{\frac{1}{3}} \tag{3.17}$$

$$H = \rho c_p \left[\frac{kzu_*\varepsilon_\theta}{\Phi_{\varepsilon_\theta}\left(\frac{z}{L}\right)}\right]^{\frac{1}{2}} \tag{3.18}$$

However, the useful application of this approach rests on the accuracy of the empirical functions Φ_ε and $\Phi_{\varepsilon_\theta}$. For the classical interpolation-type models of Φ_ε and $\Phi_{\varepsilon_\theta}$, the flux estimation demands an iterative technique, as (3.17) and (3.18) are coupled in a way that does not submit to a closed form solution. Such a scheme typically starts at an assumption of neutral conditions ($-z/L$=0), thus providing estimates Φ_ε and $\Phi_{\varepsilon_\theta}$, and in turn estimates of u_* and H. These fluxes provide an improved estimate of $-z/L$, which yields new values of Φ_ε and $\Phi_{\varepsilon_\theta}$, toward revised estimates of the fluxes, and so on iteratively.

Deacon (1959) was the first to suggest that fluxes (u_* and H) could be estimated from dissipation rates, but he did not actually employ the technique and he cautioned that it may not work well for strongly unstable stratifications. He mentioned that a similar approach could be used for evaporation but that its use would be limited by the lack of instruments capable of making fast measurements of water vapor concentration fluctuations. The dissipation method has since been used, mostly, over the ocean environment, with instrumentation on ships or buoys, (e.g. Fairall and Larsen, 1986; DeLeonibus and Simpson, 1987; Skupniewicz and Davidson, 1991; Edson et al., 1991). However, aircraft based data were used by Durand et al. (1991) and land based, point instrumentation were used by Hicks and Dyer (1974), Kader and Yaglom (1990) and Marsden et al. (1993). Hill et al. (1992) used optical scintillation methods over land surface path lengths of 150 meters. Others who have used scintillation methods for fluxes include Andreas (1988) and Hill et al. (1992). In a fascinating study, Raman lidar derived dissipation rates of humidity variance were used to estimate the surface flux of water vapor by Eichinger et al. (1993).

With the new three sublayer model for the dissipation rates of TKE and scalar variance, we proceed to present a model for calculating the fluxes of momentum, sensible heat and latent heat from inertial subrange estimates of the dissipation rates. The derivation of this new method is presented only briefly here. Essentially, the approach grew out of the need to produce a more accurate determination of fluxes from dissipation rates.

Sensible heat flux

As the vertical heat flux vanishes in the neutral limit of the DSL, we focus our model development on the convectively scaled power law of (3.16b) and (3.16c). It seems reasonable to apply this single form over the full range of unstable stratification. This form is appropriate wherever the heat flux is significant (i.e. $-z/L > 0$). A test of this assumption is provided below. Using the definitions of $\Phi_{\varepsilon_\theta}$, Θ_*, and L we may write

$$\begin{aligned}\Phi_{\varepsilon_\theta} &= \frac{\varepsilon_\theta kzu_*}{<w\theta>^2} = B\left(-\frac{z}{L}\right)^{-\frac{1}{3}} \\ &= B\left(\frac{g}{\Theta}\right)^{-\frac{1}{3}}\left[\frac{u_*}{<w\theta>^{\frac{1}{3}}}\right](kz)^{-\frac{1}{3}}\end{aligned} \tag{3.19}$$

where B is a single empirical constant. This convective form provides a closed form expression for the sensible heat flux

$$H = B^{-\frac{3}{5}}\rho c_p\left(\frac{g}{\Theta}\right)^{\frac{1}{5}}(kz)^{\frac{4}{5}}\varepsilon_\theta^{\frac{3}{5}} \tag{3.20}$$

This method provides a simple and direct computation of sensible heat flux, which does not require iteration or depend on u_*. Below, we will describe how to compute ε_θ.

Latent heat flux

Assuming similarity of scalars (see Brutsaert, 1982), we can extend our temperature analysis to water vapor. In fact, it is reasonable to believe that the result obtained for $\Phi_{\varepsilon_\theta}$ would apply to any scalar. Therefore, we write the normalized dissipation rate for water vapor as

$$\begin{aligned}\Phi_{\varepsilon_q} &= \frac{\varepsilon_q kz}{q_*^2 u_*} = \frac{\varepsilon_q kzu_*}{<wq>^2} = B\left(-\frac{z}{L}\right)^{-\frac{1}{3}} \\ &= B\left(\frac{g}{\Theta}\right)^{-\frac{1}{3}}\left[\frac{u_*}{<w\theta>^{\frac{1}{3}}}\right](kz)^{-\frac{1}{3}}\end{aligned} \tag{3.21}$$

This convective scaling form yields the following expression for evaporation

$$E = \rho\left[B^{-1}\left(\frac{g}{\Theta}\right)^{\frac{1}{3}} <w\theta>^{\frac{1}{3}}(kz)^{\frac{4}{3}}\varepsilon_q\right]^{\frac{1}{2}} \tag{3.22}$$

where $<w\theta>$ is taken in this case from the above calculation based on ε_θ. The dissipation rate for humidity variance can be calculated by the methods described below for temperature with the substitution of q for θ.

Momentum flux

For true convective scaling the dissipation rates of the TKE and scalar variances are independent of u_*, and so measurements of the dissipation rates do not contain the information necessary to estimate u_*. For neutral stratification the normalized dissipation rate of TKE is a constant. This neutral behavior for Φ_ε seems to continue up to about $-z/L = 0.1$ (Albertson et al., 1996). In this limited region we may use

$$\Phi_\varepsilon = \frac{\varepsilon kz}{u_*^3} = C$$

and on rearrangement

$$u_* = \left[C^{-1}\varepsilon kz\right]^{\frac{1}{3}} \tag{3.23}$$

The momentum flux per unit mass is simply $-u_*^2$. For larger values of $-z/L$ we can compute u_* from the empirical interpolation form of Φ_ε as used by WC71 (i.e. (3.11b)) with H taken from (3.20) for use in calculating L. Note this requires some iteration. Our main focus here is in estimating sensible and latent heat (water vapor) fluxes and, therefore, we will not extend the u_* model any further.

In the next section, we review several inertial subrange methods for computing ε and ε_θ from velocity and temperature fluctuation measurements.

3.1.6 Inertial range methods of determining dissipation rates

We review three methods for determining dissipation rates from inertial subrange scaling in the spirit of Kolmogorov (1941): power spectra, second order structure functions, and third order structure functions.

Spectral method

The dissipation rates (ε and ε_θ) have been determined most frequently from the one-dimensional power spectra in the inertial subrange using (Kolmogorov, 1941; Corrsin, 1951)

$$E_u(k) = \alpha_u \varepsilon^{\frac{2}{3}} k^{-5/3} \tag{3.24}$$

and

$$E_\theta(k) = \beta_\theta \varepsilon^{-\frac{1}{3}} \varepsilon_\theta k^{-\frac{5}{3}} \tag{3.25}$$

where α_u and β_θ are empirical constants that have been determined from experiments to be about 0.55 and 0.8, respectively (McBean et al., 1971; Antonia et al., 1979; Kaimal and Finnigan, 1994). Thus, the dissipation rates can be obtained from (3.24) and (3.25) evaluated at one or more wavenumbers (k) using measured spectral densities in the inertial subrange. This is the approach adopted by most researchers, who have made flux estimates from dissipation rates over oceans and land, (e.g. Hicks and Dyer, 1972; Fairall et al., 1990; Skupniewicz and Davidson, 1991; Kader, 1992; and Eichinger et al., 1993).

The power spectra method is subject to errors introduced by the jumpiness of the spectra, the data treatment required for Fourier analysis (e.g. windowing and tapering), and from the uncertainty of the constants α_u and β_θ. The dissipation rate for sensible heat computed from (3.25) is potentially more erroneous than that for TKE, as the former is dependent on an estimate (with all the attendant problems) of the latter.

Second order structure function

The second order structure function represents the averaged squared differences in a flow variable over spatial separation r in the direction of flow. For longitudinal velocity $D_{uu}(r) =< (u(x+r) - u(x))^2 >$ and for temperature $D_{\theta\theta}(r) =< (\theta(x+r) - \theta(x))^2 >$ (see Monin and Yaglom, 1975). These terms scale in the inertial subrange according to Kolmogorov (1941; for velocity) and Obukhov (1949; for temperature) as

$$D_{uu}(r) = C_{uu} \varepsilon^{\frac{2}{3}} r^{\frac{2}{3}} \tag{3.26}$$

$$D_{\theta\theta}(r) = C_{\theta\theta} \varepsilon_\theta \varepsilon^{-\frac{1}{3}} r^{\frac{2}{3}} \tag{3.27}$$

where $C_{uu}(= 4.0\alpha_u)$ and $C_{\theta\theta}(= 4.0\beta_\theta)$ are empirical constants (Anselmet et al., 1984). From these equations the dissipation rates can be computed, using values of the constants taken from the literature. This approach was used by Taylor (1961) in perhaps the first application of the inertial-dissipation method. However, due to the uncertainty in these empirical constants, there is some degree of imprecision in this approach as well.

Third order structure function

For velocity the third order structure function represents the averaged cubed velocity differences over lag r, $D_{uuu}(r) =< (u(x+r) - u(x))^3 >$ (Monin and Yaglom, 1975, Ch.8). For temperature the mixed third order structure function is $D_{u\theta\theta} =< (u(x+r) - u(x))(\theta(x+r) - \theta(x))^2 >$. These structure functions scale in the inertial subrange with r as

$$D_{uuu}(r) = -\frac{4}{5}\varepsilon r \tag{3.28}$$

$$D_{u\theta\theta}(r) = -\frac{4}{3}\varepsilon_\theta r \tag{3.29}$$

Note that with this approach the dissipation rates for momentum and heat can be directly computed without resort to empirical constants. This method is superior to the second order methods in that no empirical constants are used and also the dissipation rate for temperature variance is not dependent on prior numerical calculation of the dissipation rate for momentum. This approach has been used by Albertson et al. (1996) for momentum, and by Kiely et al. (1996) for heat. The application of dissipation rates derived by third order structure functions to compute fluxes is shown below.

3.2 Experiments

Surface energy balance and atmospheric turbulence measurements were carried out in the summer of '94, at two sites in California (Albertson et al., 1996; Kiely et al., 1996). One was located at the Campbell Tract research facility at the University of California at Davis in the Central Valley of California and the second was at a dry lake bed at Owens Valley in southeastern California. Eddy correlation equipment consisted of a one dimensional sonic anemometer with a fine wire (dia. = 0.0127 mm) thermocouple and a Krypton hygrometer operating at 10 Hz, with covariances taken over 20 minute averaging periods. This enabled the direct measurement of the vertical fluxes of sensible and latent heat. A three-dimensional sonic anemometer was used to record the three velocity components at 21 Hz for the Campbell Tract site and 56 Hz for the Owens Lake site. Instantaneous air temperature was also measured from the speed of sound recorded by the 3-D sonic. From the 3-D sonic we obtain direct measurements of u_* (and so the flux of momentum). The eddy correlation equipment ran continuously for the experimental duration (six weeks at Davis and two weeks at Owens Lake) with data logged on 20 minute time increments. Typically, the 3-D sonic ran for up to 12 hours per day and the data recorded to a new file every 20 minutes (i.e. 25200 data points at 21 Hz and 67200 points at 56 Hz) to match the eddy correlation and energy balance time steps.

The Davis site is a flat bare soil field of 500 m by 500 m extent. In the northeast corner of the field an irrigated portion extends 155 m in a north-south line and 115 m in an east-west line. The surface roughness length is z_0 = 2 mm. The fetch for uniform surface roughness exceeded 400 m and for surface wetness the fetch exceeded 100 m. The experiments were performed in June and July, with daytime highs of about 30°C and nighttime lows of about 15°C. The 3-D sonic anemometer was set at z=0.85 m for the initial 4 days and at z=1.5 m thereafter. Irrigations were performed at the beginning of the experiment and also three weeks later. The three week period in between was dry, with no recorded rain. By saturating the soil surface most of the available energy was forced to latent heat rather than to sensible heat, thus extending the range of near neutral flows encountered. Throughout the experiment

a wide range of atmospheric stabilities were observed with low $-z/L$ values during the days immediately following irrigation and increasingly large values as the drying out of the bare soil continued and more of the available energy was forced to sensible heat.

The dry Owens Lake site, which had daytime highs of about 40°C and night-time lows of about 15°C during August 1994, enabled investigation over a wider range of convective atmospheric conditions than in Davis. Owens Lake is an arid flat landscape with uniform fetch exceeding 10 km, and a lakebed area of about 200 km^2. The surface roughness length of the lakebed has been estimated at $z_0 = 0.13$ mm (Katul et al., 1995b). The 3-D sonic anemometer was set at z=2.65 m, and data were recorded at 56 Hz.

3.3 Dissipation Results

3.3.1 Data screening

Of the collected data, 180 files (each of 20 minute duration) were selected for analysis. The selection was based on a requirement that the files support unambiguous decomposition into means and fluctuations and that they possess turbulence intensity values ($T.I. = \sigma_u / < U >$) of less than 50%, as necessary for the application of Taylor's hypothesis (Stull, 1988). The Davis experiment contributed 105 of these files and Owens Lake the remainder. The atmospheric stability range encountered was $0.004 < -z/L < 8.1$. For each file the power spectra of the longitudinal velocity and temperature were computed using square windowing of 2048 points, bell tapering the first and last 10% of the window (Stull, 1988, p.309), using an FFT to compute the spectra of the window, repeating the process on the remaining windows and averaging all windows for each wavenumber. The power spectra of w was also calculated for each file to verify local isotropy, which is necessary for inertial subrange scaling and is indicated by $\frac{E_w}{E_u} = \frac{4}{3}$ (Tennekes and Lumley, 1972).

Typical power spectra of velocity and temperature are shown in Figures 3.4a, and 4b. These spectra have been frequency smoothed for presentation; in their original form they are quite jumpy. Note that they follow the expected -5/3 scaling over a wide range of wavenumbers. Typical second order structure functions for velocity and temperature are shown in Figures 3.5a and 5b. As expected they both follow the 2/3 scaling. Figures 3.6a and 6b are typical velocity and temperature third order structure functions. They both follow the r^1 scaling for the short lag portion which is expected to scale inertially. The third order structure functions are considered to be a more stringent test of the inertial subrange (Katul et al., 1995a). The second and third order structure functions do not require smoothing as the time averaging process provides stable measures that vary smoothly with r.

3.3.2 Normalized dissipation rates for TKE

From the computed power spectra, log transformation of (3.24) allows the straightforward determination of ε from the regressed intercept of $\log(E)$ vs $\log(k)$. A similar approach to the second order structure function provides an estimate of ε. Due to the uncertain nature of the actual values of α_u and S_2 and the susceptibility of power spectra and the second order structure function to intermittency effects on the inertial subrange scaling, we place more confidence in the third order structure function. A comparison of the three methods was made by Albertson et al. (1996). Here we focus on the third order approach and compute ε from (3.28). For the third order structure function, the Φ_ε results for the 180 data files are binned in equal log increments of $-z/L$ and presented in Figure 3.7. The scaling forms of (3.12) were fit to the

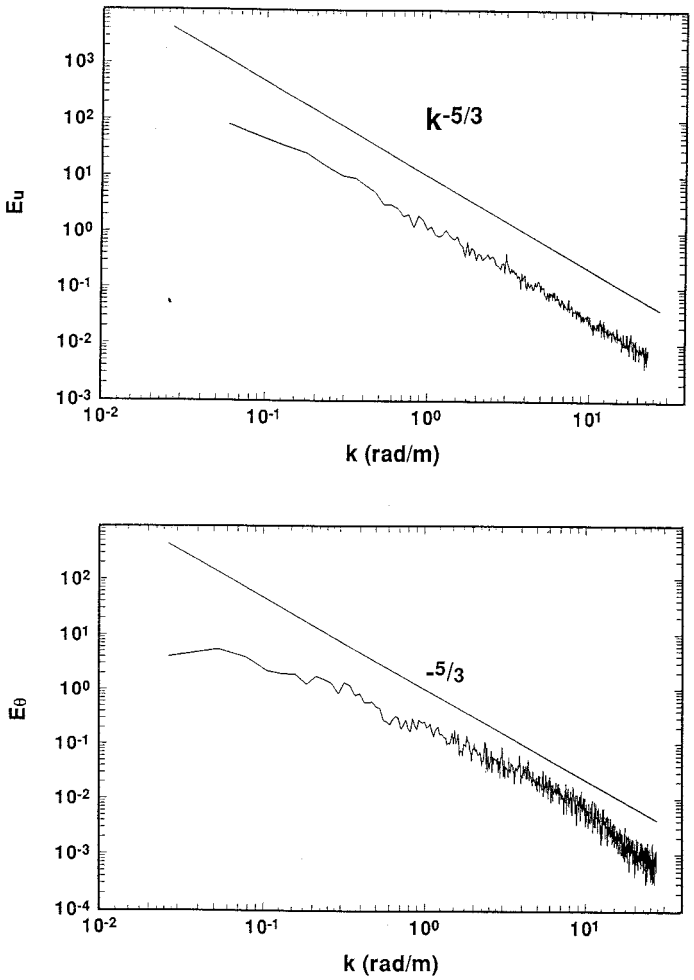

Figure 3.4: *(a) Sample power spectrum of longitudinal velocity from one of the measured 3D sonic files (top). (b) Sample power spectrum of temperature fluctuations (bottom).*

unbinned third order structure function based dissipation estimates of Albertson et al. (1996), resulting in

$$\Phi_\varepsilon = 0.61 \qquad -\frac{z}{L} < 0.04 \tag{3.30a}$$

$$\Phi_\varepsilon = 0.35\left(-\frac{z}{L}\right)^{-\frac{1}{3}} + 2.28\left(-\frac{z}{L}\right) \qquad 0.12 < -\frac{z}{L} < 1.2 \tag{3.30b}$$

$$\Phi_\varepsilon = 1.81\left(-\frac{z}{L}\right) \qquad -\frac{z}{L} > 2.0 \tag{3.30c}$$

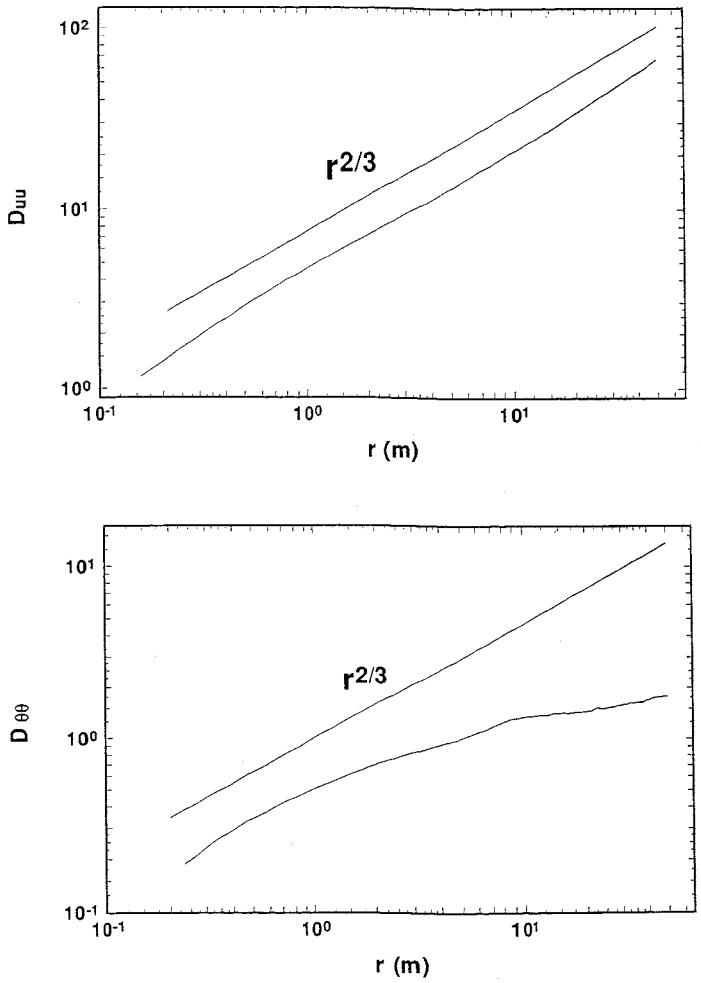

Figure 3.5: *(a) Sample second order structure function of longitudinal velocity (top). (b) Sample second order structure function of temperature fluctuations (bottom).*

These are shown by a solid line in Figure 3.7, with production represented by $[(1-16\,|z/L|)^{-1/4} - z/L]$ and the normalized dissipation model of WC71 is shown for comparison. It is clear from our results in Figure 3.7, that in the DSL the dissipation rate is significantly less than production, in the DCSL the dissipation rate is about equal to production, and in the FCSL the dissipation rate slightly exceeds production. We present (3.30) as a scaling form for TKE dissipation rates based on the three sublayer model.

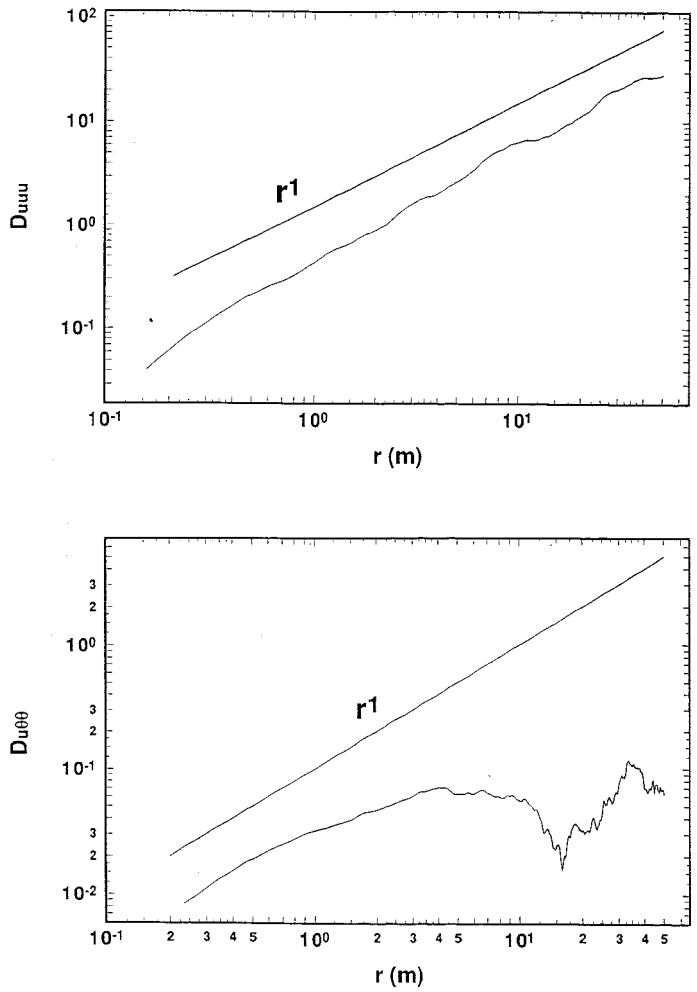

Figure 3.6: *(a) Sample third order structure function of longitudinal velocity (top). (b) Sample mixed third order structure function of velocity and temperature fluctuations (bottom).*

3.3.3 Normalized dissipation rates of temperature

From the temperature spectra, log transformation of (3.25) allows the straightforward determination of ε_θ from the regressed intercept of log (E_θ) vs log(k), with ε known from the above analysis. A similar approach to the second order structure function provides an estimate of ε_θ. Due to the uncertainty associated with the constants in the spectral and the second order structure function methods (Kiely et al., 1996), we determine the constants for (3.16) using only the third order structure function (3.29) based results. A comparison of the three inertial subrange methods was made by Kiely et al. (1996). The three sublayer model for $\Phi_{\varepsilon_\theta}$ (3.16) was

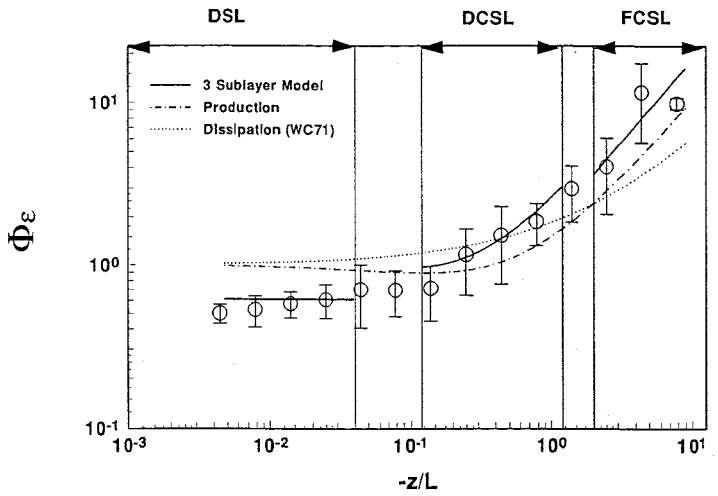

Figure 3.7: *Dimensionless TKE dissipation function plotted vs. the stability parameter -z/L. The circles represent the mean values of the data in each bin and the bars denote +/- one standard deviation of the data in the bins. The dissipation rates were computed from the third order structure functions. The fit 3 sublayer model is shown with a solid line. The normalized production is shown with dot-dash and the dissipation model of WC71 is shown with a dotted line.*

least squares fit to the unbinned third order structure function derived dissipation results, and resulted in the following model (Kiely et al., 1996)

$$\Phi_{\varepsilon_\theta} = 0.88 \qquad -\frac{z}{L} < 0.04 \tag{3.31a}$$

$$\Phi_{\varepsilon_\theta} = 0.11\left(-\frac{z}{L}\right)^{-\frac{1}{3}} \qquad 0.12 < -\frac{z}{L} < 1.2 \tag{3.31b}$$

$$\Phi_{\varepsilon_\theta} = 0.11\left(-\frac{z}{L}\right)^{-\frac{1}{3}} \qquad -\frac{z}{L} > 2.0 \tag{3.31c}$$

which is shown in Figure 3.8 along with the Businger-Dyer model of production. The dimensionless dissipation rate scales with a single convective power law over an extended range of $-z/L$, thus simplifying greatly the calculation of sensible heat flux from ε_θ and supporting the application of the single power law for flux calculations over the entire range of $-z/L > 0$. This is similar to the extended convective scaling found for the standard deviation of temperature fluctuations (e.g. Albertson et al., 1995a).

3.4 Dissipation-Flux Model

Recall that the pitfalls in the traditional spectral or second order structure function dissipation methods have been described to include: the uncertainty of the empirical constants for the second order subrange scaling of velocity and scalars; the requirement of a two step process of

first estimating ε from u and then ε_θ from ε and inertial subrange scaling of θ; possible errors due to the jumpiness of the spectra when examined over a narrow range of wavenumbers; and, the need for an iterative solution of heat fluxes. We avoid all of these problems with the present approach.

With the application of third order structure functions and the use of Taylor's hypothesis we may obtain estimates of the dissipation rates from single lag values of the structure functions

$$\varepsilon = -\frac{5}{4}\frac{D_{uuu}(\tau)}{\tau U} \tag{3.32a}$$

$$\varepsilon_\theta = -\frac{3}{4}\frac{D_{u\theta\theta}(\tau)}{\tau U} \tag{3.32b}$$

$$\varepsilon_q = -\frac{3}{4}\frac{D_{uqq}(\tau)}{\tau U} \tag{3.32c}$$

where $\tau(=r/U)$ is the time lag corresponding to r. Note that τ must be chosen to correspond to spatial lags that fall in the inertial subrange. We write the flux equations for the sensible heat and evaporative fluxes by making the substitution of (3.32) into (3.20) and (3.22) to obtain

$$H = (0.11)^{-\frac{3}{5}}\rho c_p\left(\frac{g}{\Theta}\right)^{\frac{1}{5}}(kz)^{\frac{4}{5}}\left[-\frac{3}{4}\frac{D_{u\theta\theta}(\tau)}{\tau U}\right]^{\frac{3}{5}} \tag{3.33a}$$

$$E = \rho\left[(0.11)^{-1}\left(\frac{g}{\Theta}\right)^{\frac{1}{3}} < w\theta >^{\frac{1}{3}}(kz)^{\frac{4}{3}}\left[-\frac{3}{4}\frac{D_{uqq}(\tau)}{\tau U}\right]\right]^{\frac{1}{2}} \tag{3.33b}$$

where the time average in the structure functions $D_{u\theta\theta}(\tau)$ and $D_{uqq}(\tau)$ can be computed directly by a data logger for a single time lag τ. This is possible because the third order structure function is smooth enough to provide accurate estimates of the intercept from the known slope with just one point on the curve.

As described above the friction velocity may be computed for moderate values of $-z/L$ using

$$u_* = \left[C_1^{-1}\left(-\frac{5}{4}\frac{D_{uuu}(\tau)}{\tau U}\right)kz\right]^{\frac{1}{3}} \tag{3.34}$$

This approach for determining the fluxes of H, E and u_* has several advantages over the classical method of computing fluxes from dissipation rates: (i) it does not require potentially error-inducing data treatment as with the Fourier transform, (ii) it does not rely on regressions over a range of wavenumbers as needed with jumpy power spectra, (iii) it does not rely on uncertain spectral scaling constants (i.e. α_u and β_θ), and (iv) it is free of iteration.

3.5 Evaluation of Model Performance

To test the above described model we present sensible and latent heat flux estimates using the model and compare them to direct measurements from eddy correlation. The flux comparisons are for time periods not covered by the data files used to fit the dissipation rate scaling forms of Φ_ε and $\Phi_{\varepsilon_\theta}$. The sensible heat flux comparison covers a three day period during which a wide range of H was encountered. The comparison is shown in Figure 3.9. Note that the model estimates from (3.33a) match the eddy correlation measurements to within the 10% stated accuracy range for eddy correlation. The latent heat flux comparison is made for a day with fast response humidity measurements available and a wet surface, to test the model over a wide

range of LE. Only one day of data is available for this comparison. The comparison of model estimates of LE using (3.33b) to eddy correlation measurements of LE is shown in Figure 3.10. This agreement is also considered excellent.

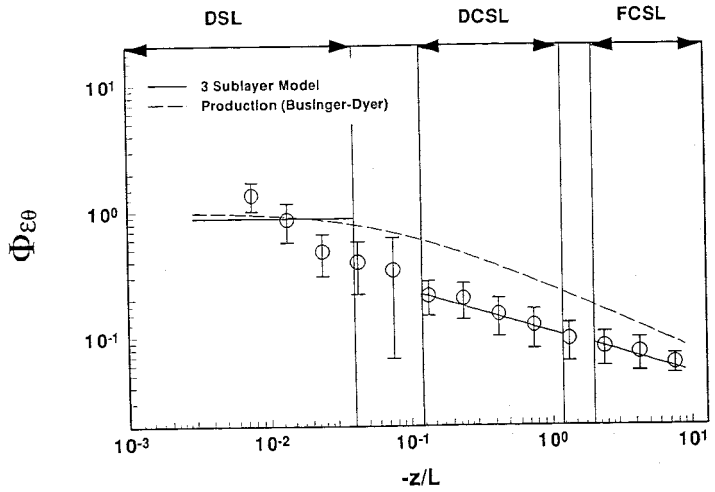

Figure 3.8: *Dimensionless temperature dissipation function plotted vs. the stability parameter -z/L. The circles represent the mean values of the data in each bin and the bars denote +/- one standard deviation of the data in the bins. The dissipation rates were computed from the mixed third order structure functions. The fit 3 sublayer model is shown with a solid line and the normalized production is shown with a dashed line.*

3.6 Discussion and Conclusions

We have presented measurements from 180 velocity/temperature files in the ASL over a wide range of atmospheric stabilities (three decade range of $-z/L$). Average dissipation rates of TKE and temperature variance were computed using third order structure functions. We place more confidence in this approach as it is devoid of empirical constants and also since the temperature dissipation rate does not require a priori knowledge of the TKE dissipation rate. These dissipation rates are evaluated in the context of the three sublayer model of Kader and Yaglom (1990). The new empirical functions developed show that in the DSL the dissipation rates of TKE are constant and therefore independent of z, and are significantly less than production. In the DCSL and in the FCSL the dissipation rates of TKE follow yet exceed production, as defined by the empirical function of Wyngaard and Coté (1971). The dissipation rate of temperature variance in our fit to the three sublayer model are shown to scale with a single convective power law over a broad range of stability.

We use these dissipation rate scaling forms to develop a simple technique for computing the fluxes of momentum, sensible heat, and water vapor, in a direct one step method. This is in contrast to the traditional, iterative dissipation approach of computing fluxes. Sensible heat flux was estimated from dissipation measurements independent of those used to fit the $\Phi_{\varepsilon_\theta}$

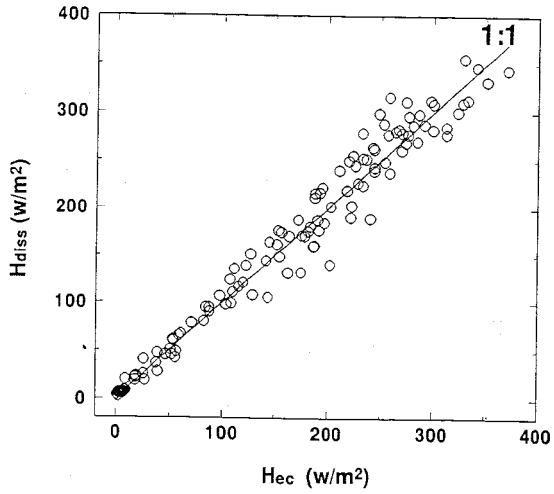

Figure 3.9: *A comparison of the sensible heat flux predictions from the presented dissipation model (H_{diss}) with direct measurements from eddy correlation (H_{ec}).*

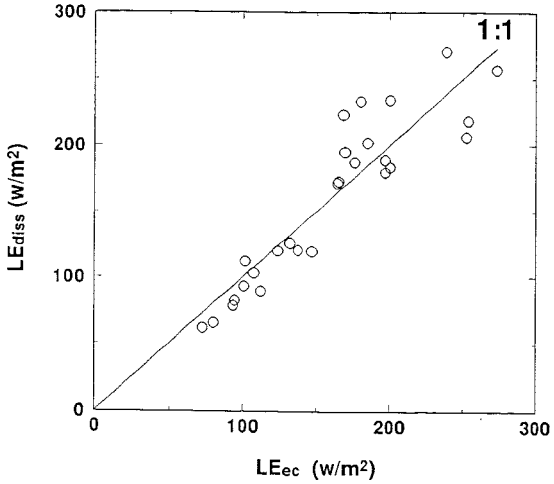

Figure 3.10: *A comparison of the latent heat flux predictions from the presented dissipation model (LE_{diss}) with direct measurements from eddy correlation (LE_{ec}).*

function. These estimates match direct measurements from eddy correlation to within the accuracy of the eddy correlation equipment. A similar comparison was made between latent heat flux estimates from the dissipation model and direct eddy correlation measurements with similarly good results.

In conclusion, we present a simple dissipation method of computing fluxes which is as accurate as the eddy correlation method, and arguably more accurate and simple than the traditional iterative dissipation approach.

Acknowledgments

The authors wish to thank Anthony Cahill and Mike Mata for their assistance in the field and Scott Tyler for his logistical help at Owens Valley. This research has been supported and financed, in part, by the National Science Foundation (EAR-93-04331), CA State Salinity Drainage Task Force, Kearney Foundation, CA Water Resources Centre (W-182), the UC Davis Superfund grant (5 P42ESO4699-07), and the NASA Graduate Student Fellowship in Global Change Research program. The support of University College Cork and the Fulbright Program is acknowledged by the Cork author.

3.7 References

Albertson JD, Parlange MB, Katul GG, Chu C-R, Stricker H, Tyler S (1995) Sensible heat flux from arid regions: A simple flux-variance method. *Water Resour Res* 31: 969–973

Albertson JD, Kiely G, Parlange MB, Eichinger WE (1996) The average dissipation rate of turbulent kinetic energy in the neutral and unstable atmospheric surface layer. *Journal of Geophysical Research*

Andreas EL (1998) Using scintillation at two wavelengths to measure path-averaged heat fluxes in free convection. *Boundary Layer Meteorol* 54: 167–182

Anselmet F, Gagne Y, Hopfinger EJ, Antonia RA (1984) Higher order velocity structure functions in turbulent shear flows. *J Fluid Mech* 140: 63–89

Antonia RA, Chambers AJ, Phong-Anant D, Rajagopalan S (1979) Properties of spatial temperature derivatives in the stmospheric surface layer. *Boundary-Layer Meteorol* 17: 101–118

Brutsaert W (1982) *Evaporation into the Atmosphere.* Kluwer Academic Publishers 299pp

Brutsaert W (1986) Catchment scale evaporation and the atmospheric boundary layer. *Water Resour Res* 22, suppl., 39S–45S

Businger JA (1966) Transfer of momentum and heat in the planetary boundary layer. *Proc Symp Arctic Heat Budget and Atmos Circulation*, Rand Corp. RM-5233-NSF, pp.305–332

Champagne FH, Friehe CA, LaRue JC, Wyngaard JC (1977) Flux measurements, flux estimation techniques, and fine-scale turbulence measurements in the unstable surface layer over land. *J Atmos Sci* 34: 515–530

Corrsin S (1951) On the spectrum of isotropic temperature fluctuations in an isotropic turbulence. *J Appl Phys* 22: 469–473

Deacon EL (1959) The measurement of turbulent transfer in the lower atmosphere. *Adv Geophys* 6: 211–228

Deacon EL (1988) The streamwise Kolmogorov constant. *Boundary Layer Meteorol* 42: 9–17

Durand P, De Sa L, Druilhet A, Said F (1991) Use of the inertial dissipation method for calculating turbulent fluxes from low-level airborne measurements. *J Atmos Ocean Tech* 8: 78–84

DeLeonibus PS, Simpson LS (1987) Dissipation observations of drag coefficients over the open ocean. *IEEE J Oceanic Eng* OE-12: 296–300

Dyer AJ (1974) A review of flux-profile relations. *Boundary-Layer Meteorol* 1: 363–372

Dyer AJ (1967) Measurements of evaporation and heat transfer in the lower atmosphere by an automatic eddy-correlation technique. *Quart J Roy Meteorol Soc* 93: 501–508

Edson JB, Fairall CW, Mestayer PG, Larssen SE (1991) A study of the inertial-dissipation method for computing air-sea fluxes. *J Geophys Res* 96C: 10689–10711

Eichinger WE, Cooper DI, Holtkamp DB, Karl RR Jr., Quick CR, Till JJ (1993) Derivation of water vapour fluxes from lidar measurements. *Boundary-Layer Meteorol* 63: 39–64

Fairall CW, Edson JB, Larsen SE, Mestayer PG (1990) Inertial-dissipation air-sea measurements: A prototype system using realtime spectral computations. *J Atmos Ocean Tech* 7: 425–453

Fairall CW, Larsen SE (1986) Inertial-dissipation methods and turbulent fluxes at the air-ocean interface. *Boundary-Layer Meteorol* 34: 287–301

Frenzen P, Vogel CA (1992) The turbulent kinetic energy budget in the atmospheric surface layer: A review and an experimental re-examination in the field. *Boundary-Layer Meteorol* 60: 49–76

Hicks BB, Dyer AJ (1972) The spectral density technique for the determination of eddy fluxes. *Quart J R Met Soc* 98: 838-844

Hill RG, Ochs GR, Wilson JJ (1992) Measuring surface layer fluxes of heat and momentum using optical scintillation. *Boundary-Layer Meteorol* 58: 391–408

Hogstrom U (1990) Analysis of Turbulence Structures in the Surface Layer with a Modified Similarity Formulation for near Neutral Conditions. *J Atmos Sci* 47: 1949–1972

Kader BA (1988) Three-level structure of an unstably stratified atmospheric surface layer. *Izv Atmos Ocean Phys* 24: 907-919 (English translation)

Kader BA (1992) Determination of momentum and heat fluxes by spectral method. *Boundary-Layer Meteorol* 61: 323–347

Kader BA, Perepelkin VG (1984) Profiles of the mean velocity and temperature in the near surface layer of the atmosphere under conditions of neutral and unstable stratification. *Izv Atm Ocean Phys* 20: 112–119. (English Translation)

Kader BA, Yaglom AM (1990) Mean fields and fluctuation moments in unstably stratified turbulent boundary layers *J Fluid Mech* 212: 637–662

Kaimal JC, Finnigan JJ (1994) *Atmospheric Boundary Layer Flows: Their Structure and Measurement*, Oxford University Press 289pp

Katul GG, Parlange MB, Albertson JD, Chu C-R (1995a) Local isotropy and anistropy in the sheared and heated atmospheric surface layer. *Boundary-Layer Meteorol* 72 123–148

Katul GG, Chu C-R, Parlange MB, Albertson JD, Ortenburger TA (1995b) The large scale spectral characteristics of stratified atmospheric surface layer flows. *J Geophys Res*, in press

Kiely G, Albertson JD, Parlange MB, Eichinger WE (1996) On the scaling of the average dissipation rate of temperature variance in the atmospheric surface layer. *Boundary-Layer Meteorol*, submitted

Kolmogorov AN (1941) The local structure of turbulence in incompressible viscous fluid for very large Reynolds number *Dokl Akad Nauk SSSR* 30: 301–305

Leavitt E, Paulson CA (1975) Statistics of surface layer turbulence over the tropical ocean. *J Phys Oceanogr* 5: 143–156

McBean GA, Stewart RW, Miyake M (1971) The turbulent energy budget near the surface. *J Geophys Res* 76: 6540–6549

McBean GA, Elliott JA (1975) The vertical transport of kinetic energy by turbulence and pressure in the boundary layer. *J Atmos Sci* 32: 753–766

Marsden RF, McBean GA, Proctor BA (1993) Momentum and sensible heat fluxes calculated by the dissipation technique during the Ocean Storms Project. *Boundary-Layer Meteorol* 63: 22–38

Monin AS, Yaglom AM (1975) *Statistical Fluid Mechanics* Vol. II, J. Lumley (Ed.), MIT Press, 874pp

Obukhov AM (1949) Structure of the temperature field in a turbulent flow. *Izv Akad Naul SSSR, Ser Georgr i Geofiz* 13: 58–69

Panton RL (1984) *Incompressible Flow*, Wiley-Interscience, 780pp

Parlange MB, Eichinger WE, Albertson JD (1995) Regional scale evaporation and the atmospheric boundary layer. *Reviews of Geophysics* 33: 99–124

Skupniewicz CE, Davidson KL (1991) Hot-film measurements from a small buoy: Surface wind estimates using the inertial dissipation method. *J Atmos Ocean Tech* 8: 309–322

Stull R (1988) *An Introduction to Boundary Layer Meteorology*, Kluwer Academic Press, 666pp

Taylor RJ (1961) A new approach to the measurement of turbulent fluxes in the lower atmosphere. *J Fluid Mech* 10: 449–458

Tennekes H, Lumley J (1972) *A First Course in Turbulence*, MIT Press, 300pp

Wyngaard JC, Coté OR (1971) The budgets of turbulent kinetic energy and temperature variance in the atmospheric surface layer. *J Atmos Sci* 28: 190–201

Further Reading

Brutsaert W (1982) *Evaporation into the Atmosphere.* Kluwer Academic Publishers, 299pp

Parlange MB, Eichinger WE, Albertson JD (1995b) Regional scale evaporation and the atmospheric boundary layer. *Reviews of Geophysics* 33: 99–124

Stull R (1988) *An Introduction to Boundary Layer Meteorology.* Kluwer Academic Press, 666pp

Wyngaard JC (1990) Scalar fluxes in the planetary boundary layer - Theory, modeling, and measurement. *Boundary-Layer Meteorol.* 50: 49–75

Chapter 4

Introduction to Numerical Weather Prediction Data Assimilation

Phillipe Courtier
ECMWF, Shinfield Park
Reading, Berkshire RG2 9AX
UK

4.1 The Problem

In numerical weather prediction data assimilation consists of the process which estimates the initial conditions of the forecast using all the available information. A description of the current observing system can be found in McGrath (1993); around 105 elementary pieces of information are currently used over 24 hours by the operational data assimilation system.

The current operational ECMWF model (Simmons, 1991) has a horizontal resolution of 90 km and covers the whole globe. On the vertical the atmosphere is sampled with 31 levels from the surface up to 10 hPa. The number of degrees of freedom of the model is then of the order of 10^7.

Over 24 hours, the estimation problem is clearly underdetermined. The time dimension is thus a critical element of any data assimilation system: it is essential to carry forward in time information from past observations using the forecast model since it is the best information propagator available.

We have identified the main difficulties of data assimilation:

- large dimension problem
- time dimension critical but non linear dynamic
- observations of variable nature and quality

The purpose of this paper is to provide the theoretical basis of the algorithms used in operational meteorology together with some recent developments. Most of the material presented here is well documented in the meteorological literature (Lorenc, 1986; Ghil and Manalotte-Rizzoli, 1991; Daley, 1991) or in other fields under the generic name of inverse problems (Tarantola, 1987).